JAAS

ROYAL SOCIETY OF CHEMISTRY

PAPER

View Article Online
View Journal | View Issue

Cite this: *J. Anal. At. Spectrom.*, 2022, **37**, 358

Two reliable calibration methods for accurate *in situ* U–Pb dating of scheelite†

Yanwen Tang, *[a] Junjie Han,[a] Tingguang Lan,*[a] Jianfeng Gao,[a] Liang Liu,[a] Changhao Xiao[b] and Jiehua Yang[a]

Scheelite is an important metallic mineral in W-related hydrothermal deposits and can be utilized as a reliable geochronometer to directly date the timing of mineralization. Up to now, two previous studies have performed *in situ* U–Pb dating of scheelite using NIST glasses as reference materials due to the lack of scheelite standards. However, there exists a significant matrix effect between NIST612 and scheelite based on our analysis. Therefore, two reliable calibration methods have been proposed and assessed *via* LA-SF-ICP-MS in this study. A laser spot size of 32 μm was mainly used to satisfy the signal for ^{206}Pb, ^{207}Pb, and ^{238}U and keep a high resolution to fit small grains and altered crystal zones of scheelite samples. Scheelite WX27 as a secondary standard has been accurately determined in normal ablation settings of 3 J cm^{-2} – 5 Hz, 3 J cm^{-2} – 10 Hz, 5 J cm^{-2} – 5 Hz (using a spot size of 24 μm), 5 J cm^{-2} – 10 Hz, and 10 J cm^{-2} – 5 Hz. Its lower intercept ^{206}Pb/^{238}U ages are consistent with each other within error and agree with two known ages (144.8 ± 11.7 and 141.8 ± 5.3 Ma) from the Woxi deposit with age offsets of <3.8%, no matter whether they were calibrated by using concordant wolframite YGX or the combined calibration method (*i.e.*, NIST612 for ^{207}Pb/^{206}Pb and YGX for ^{238}U/^{206}Pb ratios). Moreover, accurate U–Pb ages, ranging from 432 Ma to 92 Ma, were also obtained for five typical W deposits. All these age results demonstrate the reliability of the two calibration methods and indicate that no matrix effect exists between scheelite and wolframite using single spot analysis mode in normal ablation settings. When all the same data from scheelite WX27 were calibrated by using NIST 612, most of the obtained ages were much younger than the known ages, with the age offsets ranging from 5.9% to 18.0%. Thus, NIST glasses are commonly not suitable as primary standards for *in situ* U–Pb dating of scheelite. Scheelite WX27 contains relatively high U (averaging 7.1 ppm) and low common-lead and is suitable as a candidate reference material for *in situ* U–Pb dating of scheelite at the moment.

Received 8th November 2021
Accepted 4th January 2022

DOI: 10.1039/d1ja00387a

rsc.li/jaas

1. Introduction

As an important strategic metal in the world, W deposits have attracted increasing attention recently. Scheelite is one of the metallic minerals in W-related hydrothermal deposits and can be utilized as a reliable geochronometer to directly date the timing of mineralization. The Sm–Nd isochronal age of scheelite was already reported twenty years ago,[1] and several accurate Sm–Nd isochron ages (consistent with the formation age of ore-related granite within error) were obtained to constrain the timing and origin of W mineralization.[2–5] However, the accurate U–Pb age for scheelite using isotope dilution-thermal ionization mass spectrometry has not been reported yet. Such two dating methods using bulk samples are commonly time-consuming and easily affected by the presence of U- and Pb-rich micro-inclusions or the alteration phases in which the closure of Sm–Nd and U–Pb isotope systems could be changed. Particularly, laser ablation inductively coupled plasma mass spectrometry (LA-ICP-MS) U–Pb dating of scheelite is commonly characterized by higher efficiency and spatial resolution and lower cost, and will become another important dating method for W-related deposits.

Non-matrix matched calibrations have several successful applications in LA-ICP-MS analysis, *e.g.*, NIST 610, NIST 612, and zircon 91500 as an external standard for *in situ* U–Pb dating of allanite, monazite, xenotime, cassiterite, and wolframite, respectively.[6–10] However, attributed to the different ablation behaviors, significant matrix effects have been observed in most calibration processes mentioned above and some special analyzed conditions (*e.g.*, keeping the ^{206}Pb/^{238}U ratio of NIST 610 at ~0.22 in the whole experimental process[9] or adding some water vapor by using special equipment[10]) have been applied to reduce the matrix

[a]*State Key Laboratory of Ore Deposit Geochemistry, Institute of Geochemistry, Chinese Academy of Sciences, Guiyang, 550081, China. E-mail: tyw_xt@126.com; lantingguang@126.com*

[b]*Laboratory of Dynamic Diagenesis and Metallogenesis, Institute of Geomechanics, Chinese Academy of Geological Sciences, Beijing 100081, China*

† Electronic supplementary information (ESI) available. See DOI: 10.1039/d1ja00387a

effects.[7–11] Moreover, low laser sampling rate (~3 Hz) and energy density (<3 J cm^{-2}), short ablations (~30 s, avoiding the formation of deep craters), and large crater diameters (>32 μm) were considered for *in situ* U–Pb dating to minimize matrix effects.[7,12,13]

Due to the lack of matrix-matched standards, *in situ* U–Pb dating of scheelite has been applied in two previous studies using NIST glasses as reference materials.[14,15] From these two studies, the characteristics of scheelite samples, *i.e.*, relatively high and variable radiogenic U concentrations (<1 to >10 ppm) and low common Pb concentrations (<0.01 ppm), offer us a new insight that scheelite is amenable to U–Pb geochronology. However, the reliability of such a U–Pb dating technique for scheelite has not been evaluated by any other dating techniques (*e.g.*, by isotope dilution-thermal ionization mass spectrometry (ID-TIMS)). Matrix effects between NIST glasses and scheelite remain unknown.

Tungstates include two basic structural types, *i.e.*, scheelite ($CaWO_4$)-type formed by large cations of Ca, Sr, Pb, and Ba, and wolframite ($(Mn, Fe)WO_4$)-type formed by small cations of Mg, Zn, Ni, Fe, and Mn.[16] Ferberite ($FeWO_4$) and hübnerite ($MnWO_4$) are an iron-rich endmember and manganese-rich endmember of wolframite, respectively. No matrix effect is observed between ferberite, hübnerite, and wolframite in our and previous studies[17] under normal analysis conditions. Thus, these known reference materials with ID-TIMS U–Pb ages, *i.e.*, wolframite MTM (334.4 ± 1.7 or 316.7 ± 5.8 Ma),[18,19] wolframite YGX (160.9 ± 0.7 Ma (ref. 17)), and hübnerite WT (95.2 ± 1.0 Ma (ref. 20)), can used to calibrate these wolframite-type minerals. However, whether these reference materials can be used to calibrate scheelite or whether matrix effects exist between scheelite and wolframite is still unclear.

In this study, several scheelite samples from five typical W deposits, with a wide range of formation ages (from 430 to 92 Ma), were selected for methodological analysis. The main objectives are (1) to evaluate the matrix effects between scheelite and NIST 612, and scheelite and wolframite in *in situ* U–Pb chronology; (2) to establish an accurate calibration method for LA-ICP-MS U–Pb dating of scheelite.

2. Experimental

2.1 Sample preparation and cathodoluminescence (CL) observation

The scheelite grains or fragments from all the samples were mainly embedded in about 1 or 1.5 cm epoxy mounts and polished.

CL images were photographed to identify the internal textures of scheelite and to help interpret their ages. A JSM-7800F field emission scanning electron microscope equipped with a Gatan MONO CL4 detector was used at the State Key Laboratory of Ore Deposit Geochemistry (SKLODG), Institute of Geochemistry, Chinese Academy of Sciences (IGCAS), Guiyang, China. The analytical conditions are listed below the CL images.

2.2 LA-SF-ICP-MS

All scheelite analyses were performed on a GeoLasPro 193 nm ArF excimer laser (CompexPro 102F, Coherent), coupled to an Element XR sector field ICP-MS (Thermo Fisher Scientific, USA) for U–Pb dating at the SKLODG, IGCAS, Guiyang, China. Smaller spot sizes were used to get higher spatial resolution due to higher sensitivity than quadrupole (Q)-ICP-MS. The standard cylinder ablation cell was optimized with a resin mold to get a smaller volume and offer a fast washout of the aerosol. Helium was used as the carrier gas. Small amounts of nitrogen (~3 mL min^{-1}) were added to the helium gas to increase the sensitivity *via* a simple Y junction downstream of the sample cell and then mixed with argon *via* a T-connector before introducing into the ICP-MS. NIST SRM 612 glass was used to maximize the ratios of the signal relative to background intensity for Pb and U when the U/Th ratios were kept at about 1.05. Samples and standards were embedded in small epoxy mounts (~1 cm) and placed together in the center to minimize the position effect. Each spot analysis incorporated an approximate 20 s background and 30 s sample data acquisition. A pre-ablation of 5–8 pulses was performed to eliminate common Pb contamination from the sample surface. Only smooth signals were saved to preclude the high common-lead effect from fluid inclusion or other minerals (*e.g.*, sulfide). The dwell times for each mass scan are 3 ms for ^{202}Hg, ^{204}Pb, ^{208}Pb, and ^{232}Th, 15 ms for ^{206}Pb and ^{238}U, and 25 ms for ^{207}Pb, respectively. The analytical conditions are summarized in Table 1.

Based on our experiences on garnet and wolframite by LA-SF-ICP-MS[21,22] and considering that we want to obtain a signal for ^{206}Pb, ^{207}Pb, and ^{238}U and keep a high resolution to fit small grains and altered crystal zones of some scheelite samples, the ablation settings, *i.e.*, a laser spot size of 32 μm (24 μm in one analytical section), repetition rates of 5 and 10 Hz, and energy densities of 3, 5, and 10 J cm^{-2}, were mainly used to analyze a relatively well-characterized scheelite sample WX27 for comparison. Normal conditions of 32 μm, 3 J cm^{-2}, and 5 Hz were applied to analyze all other scheelite samples from typical W deposits.

2.3 Calibration strategy and data reduction

The time-dependent drifts of U–Pb isotopic ratios were corrected with a standard-sample bracketing procedure, *i.e.*, 2

Table 1 Analyzed conditions for LA-SF-ICP-MS measurements

For LA-SF-ICP-MS	
Geolas Pro 193 nm laser ablation system	
Energy density	3, 5, 10 J cm^{-2}
Spot size	32 and 24 μm
Laser frequency	5, 10 Hz
Ablation cell gas	Helium (0.45 L min^{-1})
Thermo Fisher Scientific finnigan element XR ICP-MS	
Power	1230 W
Plasma gas flow rate	16.0 L min^{-1}
Auxiliary gas flow rate	About 0.95 L min^{-1}
Scan type	EScan
Dwell times (ms)	3 ms for ^{202}Hg, ^{204}Pb, ^{208}Pb, ^{232}Th; 15 ms for ^{206}Pb, ^{238}U; 25 ms for ^{207}Pb
Addition of nitrogen to increase the sensitivity	3 mL min^{-1}

NIST612 + 4 YGX + 2 MTM or/and + 2 WT + 10–15 samples + 2 WT or/and + 2 MTM + 4 YGX + 2 NIST612. Each of YGX, MTM, and WT was analyzed more than ten times in total to obtain a more accurate age in the Tera–Wasserburg Concordia diagram. As there is no homogeneous matrix-matched primary standard for scheelite, three different calibration strategies were considered as follows:

(1) Using concordant wolframite YGX as the primary standard. Yang *et al.*[17] confirmed that wolframite YGX should be characterized by high U and low common-lead, and have a concordant U–Pb age of 160.9 ± 0.7 Ma. Therefore, if the U–Pb ages of analyzed YGX spots are concordant, YGX will be taken as the primary standard to calibrate the U–Pb isotopic ratios of scheelite samples. Other samples, *e.g.*, wolframite MTM and hübnerite WT can be used as secondary standards. Targeting the area with a low $^{207}Pb/^{206}Pb$ value of <0.2 may empirically improve the possibility to obtain the concordant age for YGX due to its inhomogeneity.

(2) Using the combined calibration method, *i.e.*, NIST612 for calibrating the $^{207}Pb/^{206}Pb$ ratios and YGX for calibrating the $^{238}U/^{206}Pb$ ratios of the unknown samples. Completely homogeneous wolframite standards were not found till now. Three proposed wolframite standards of MTM, YGX, and WT are more homogeneous than others, but also have variable U and common Pb shown in the Tera–Wasserburg Concordia diagram in previous and our studies.[10,20,21,23] Moreover, they were with different ID-TIMS U–Pb ages of 334.4 ± 1.7 and 316.7 ± 5.8 Ma, 152.8 ± 2.0 and 160.9 ± 0.7 Ma, and 95.2 ± 1.0 and 104.3 ± 0.5 Ma.[17–20,23] Thus, if there are no concordant YGX spots, a combined calibration method using wolframite YGX and NIST glasses (*e.g.*, NIST612) to correct the mass fractionation of $^{238}U/^{206}Pb$ and $^{207}Pb/^{206}Pb$ isotope ratios of the unknowns, respectively, is to be used. A calibration factor, which is calculated from the measured/accepted age of wolframite YGX (accepted age 160.9 ± 0.7 Ma (ref. 17)), was used to multiply by the measured $^{238}U/^{206}Pb$ ratios of the unknowns (finished in Excel). The measured/accepted ages and $^{238}U/^{206}Pb$ ratios are obtained from the intercept values in the Tera–Wasserburg Concordia diagram as shown in Fig. S-1.†

Moreover, hübnerite WT (95.2 ± 1.0 Ma (ref. 20)) and wolframite KA (430 Ma (ref. 21)) were analyzed for quality controls and modifying the measured/accepted ratio to make sure all their ages are acceptable within error, if necessary. The initial $^{207}Pb/^{206}Pb$ ratios are 0.847 for YGX,[24] 0.851 (ref. 25) for WT, and 0.865 (ref. 26) for wolframite KA in the Tera–Wasserburg Concordia diagram.

(3) Using NIST612 as the primary standard to calibrate both of the $^{207}Pb/^{206}Pb$ and $^{206}Pb/^{238}U$ ratios of the unknowns. The data collected from ICP-MS were processed offline using the ICPMSDataCal software for trace element content and U–Pb age calibration.[27] The detailed calibration equation for age using concordant wolframite YGX or NIST 612 as the primary standard to correct both of the $^{238}U/^{206}Pb$ and $^{207}Pb/^{206}Pb$ isotope ratios has been described in previous studies[10,28] and is also provided in the ESI (Table S-1†). Excluding the beginning ~2 s, only the first ~25 s of ablation data were used in the calculation to reduce or eliminate down-hole fractionation effects. NIST612 was used as an external standard to calibrate U and Pb concentrations without applying an internal standard. Isoplot 4.15 was used to calculate and finish the Tera–Wasserburg Concordia diagram anchored through common Pb (*i.e.*, common Pb correction) to obtain the lower intercept ages. Data errors reported for isotopic ratios were 1σ. Due to inhomogeneous U/Pb ratios (varying from 2.8 to 46.2, Table S-2†) and variable common-lead, the time-dependent U–Pb fractionation of scheelite has not been shown here to explain the matrix effect in different ablation settings against other two reference materials, *i.e.*, NIST612 and wolframite YGX.

3. Samples

3.1 Wolframite YGX and hübnerite WT

Wolframite mineral YGX is from a granite-related Yaogangxian vein-type W deposit in the Nanling belt, South China. It was used as the primary standard to calibrate the U–Pb geochronology of the scheelite samples in this study. Hübnerite mineral WT from a hydrothermal Wutong deposit in the Nanling belt, South China, was used as the alternate primary standard or secondary standard. The acceptable ID-TIMS ages of samples YGX and WT are 160.9 ± 0.7 Ma (ref. 17) and 95.2 ± 1.0 Ma.[20] Wolframite YGX has been confirmed as a well-characterized U–Pb wolframite reference material in a previous study.[8]

3.2 Low common-lead scheelite sample WX27 from the Woxi giant W–Sb–Au polymetallic ore deposit

Scheelite sample WX27-12 is from quartz-vein-type ore from the Woxi giant W–Sb–Au polymetallic ore deposit in Hunan Province, China. Scheelite, stibnite, and quartz are observed in this ore sample (Fig. 1A). The W–Sb–Au mineralization event was constrained by the Rb–Sr isochronal age of 144.8 ± 11.7 Ma for fluid inclusions in quartz intergrowth with stibnite.[29] Recently, *in situ* U–Pb dating of wolframite, apatite, and scheelite was finished in our laboratory. The W–Sb–Au mineralization event was constrained by several accurate ages, including an unpublished apatite *in situ* U–Pb age of 141.8 ± 5.3 Ma (calibrated by using apatite OD306 (ref. 30) and verified by using QH apatite at ~160 Ma (ref. 31)) and two accurate scheelite *in situ* U–Pb ages of 144.3 ± 2.2 and 142.7 ± 2.4 Ma (described below). The characteristics of relatively high U and low common-lead were found and verified for scheelite WX27.

3.3 Scheelite sample KA from the super large-sized Baiganhu W–Sn ore district

The main W–Sn mineralization event of this granite-related deposit has been well constrained by *in situ* cassiterite U–Pb ages of 427 ± 13 Ma (ref. 32) and 427.6 ± 5.1 Ma,[21] *in situ* wolframite U–Pb ages of 425.9 ± 4.3 Ma and 429.2 ± 6.8 Ma,[21] and muscovite $^{40}Ar/^{39}Ar$ ages of 411.7–412.8 Ma (ref. 33) or 421.8–422.7 Ma.[34] LA-ICP-MS and SIMS U–Pb zircon dating of the spatially associated monzogranite yield the ages of 430.5 ± 1.2 Ma (ref. 32) and 421 ± 3.7 Ma,[35] respectively. Scheelite KA was collected from quartz-vein type ores, which are often composed of wolframite, cassiterite, scheelite, quartz, and muscovite.[34]

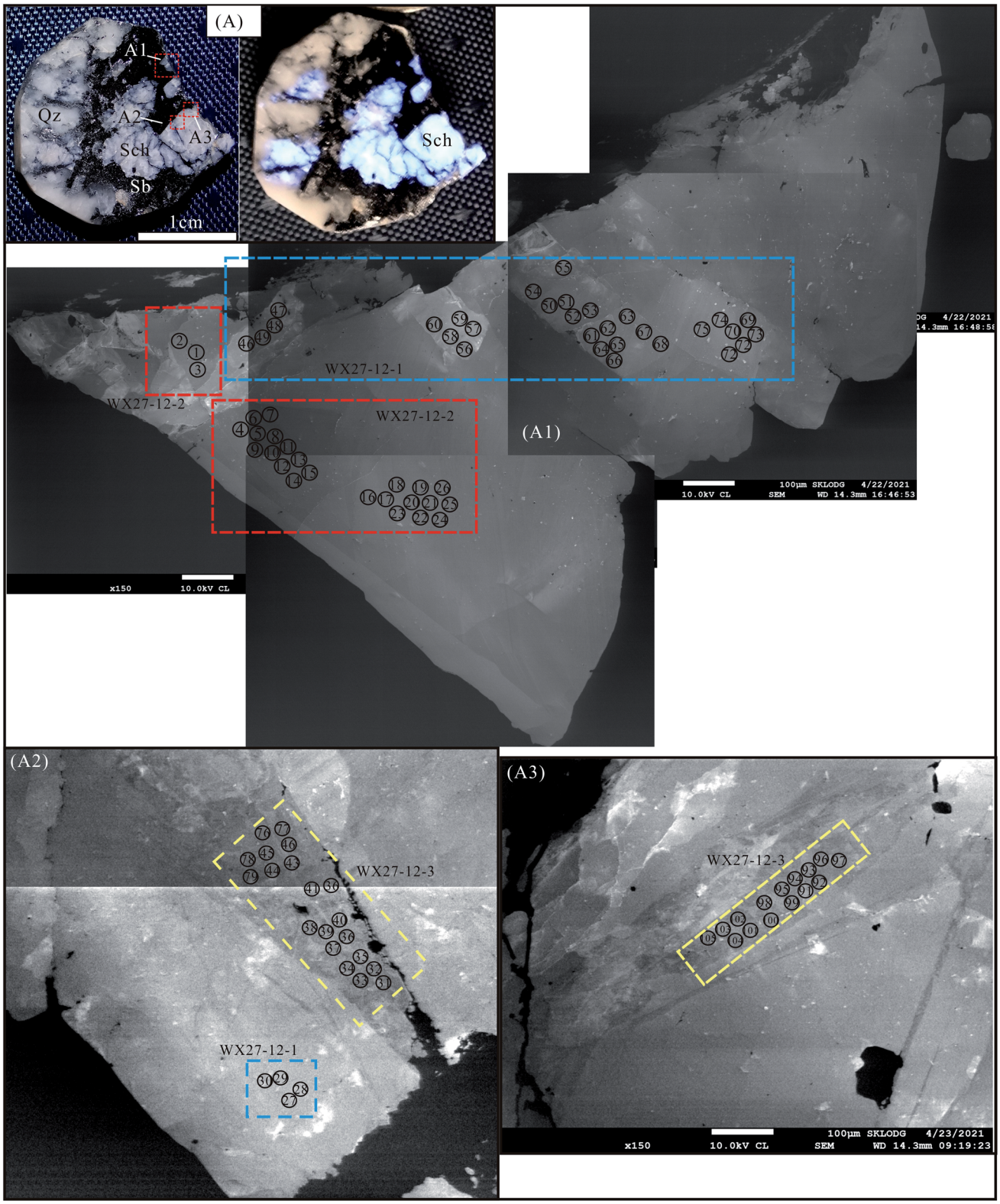

Fig. 1 The low common-lead scheelite WX27-12 from the Woxi giant W–Sb–Au polymetallic deposit. (A) Scheelite (Sch), stibnite (Sb), and quartz (Qz) coexist with each other, and three scheelite grains were photographed by cathodoluminescence (CL) and chosen for *in situ* U–Pb dating; (A1–A3) spot position for analysis, WX27-12-1 for the white zones, WX27-12-2 for the black zones, and WX27-12-3 for the late black vein with a width of 100 to 200 μm.

3.4 Scheelite sample LW from the Luowei large-sized W polymetallic ore deposit

The formation age of this deposit was constrained by muscovite $^{40}Ar/^{39}Ar$ ages of 92 ± 3 and 93 ± 3 Ma, and the molybdenite Re–Os age of 95.9 ± 1.7 Ma.[36] LA-ICP-MS U–Pb zircon dating of the spatially associated monzogranite and biotite granite yield the ages of 92.5 ± 1.1 and 92.9 ± 0.7,[37] and 98.0 ± 1.0 and 99.8 ± 0.9 Ma,[36] respectively. Scheelite sample LW coexists with molybdenite, pyrite, and quartz.

3.5 Scheelite sample YCL from the Yangchuling large-sized W–Mo deposit

The main W–Mo mineralization event of this deposit was constrained by molybdenite Re–Os ages of 144.9 ± 0.7 (ref. 38) and 146.4 ± 1.0 Ma.[39] The spatially associated intrusions were constrained by LA-ICP-MS zircon U–Pb dating at 143.8 ± 0.5, 145.1 ± 0.4, and 149.8 ± 0.6 Ma,[38,39] respectively. Scheelite sample YCL was chosen from porphyry-type ores and is characterized by disseminated euhedral and subhedral scheelite, which coexists with molybdenite locally.

3.6 Scheelite sample XLS from the Xianglushan super large-sized scheelite deposit

The formation age of this deposit was constrained by the scheelite Sm–Nd isochronal age of 121 ± 11 Ma, quartz Rb–Sr isochronal age of 128 ± 3 Ma, muscovite $^{40}Ar/^{39}Ar$ age of 122.8 ± 0.8 Ma, and molybdenite Re–Os age of 125.5 ± 0.7 Ma.[40,41] The formation age of the spatially associated biotite granite is constrained by the whole-rock Rb–Sr isochronal age of 126.2 ± 2.6 Ma (ref. 40) and LA-ICP-MS zircon U–Pb ages of 117.3 ± 1.7 and 123.8 ± 0.8 Ma.[41] Scheelite sample XLS is chosen from a quartz-scheelite-chlorite vein with ~0.5 cm thickness and characterized by disseminated euhedral and subhedral scheelite.

4. Results

4.1 Low common-lead characteristics of scheelite WX27

Two hundred and sixty-two spots were analyzed in total for scheelite WX27 in different ablation settings to check the matrix effects between wolframite and scheelite, and NIST612 and scheelite. These spots contain U concentrations varying from 0.1 to 24.6 ppm (averaging 7.1 ppm) and total Pb concentrations ranging from 0.1 to 4.8 ppm (averaging 0.3 ppm) (Table S-2†), respectively. Most of these spots were with the $^{207}Pb/^{206}Pb$ values of <0.2 and plotted near the lower intercept in the Tera–Wasserburg Concordia diagram (shown below).

4.2 U–Pb results of scheelite WX27 calibrated by using concordant wolframite YGX in different ablation settings

The normal ablation settings of low to medium energy densities (3–5 J cm^{-2}) and medium–high sampling rates (5–10 Hz), and even high energy density (10 J cm^{-2}) and medium sampling rate (5 Hz) were applied to analyze scheelite WX27. Moreover, a small spot size of 24 μm was included to combine the medium energy density (5 J cm^{-2}) and medium sampling rate (5 Hz) in

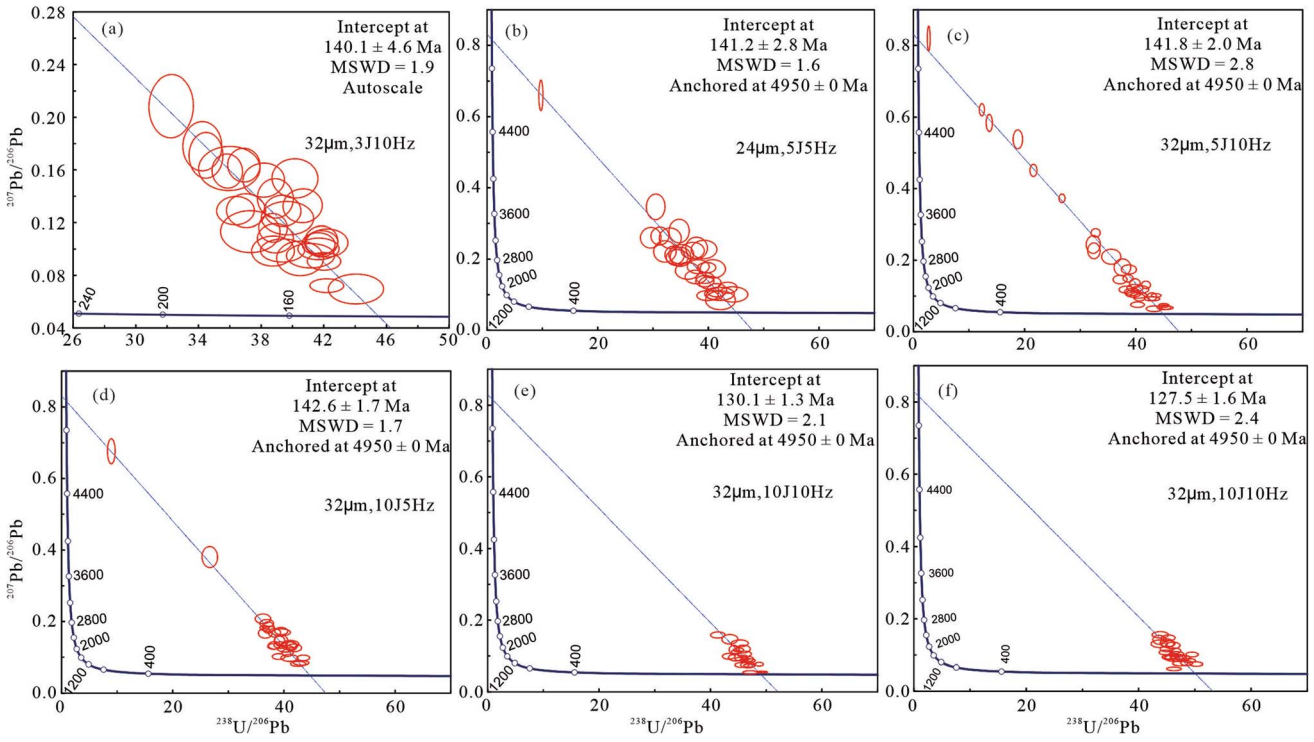

Fig. 2 *In situ* U–Pb ages of scheelite WX27 calibrated by using concordant wolframite YGX samples in different ablation settings (no concordant wolframite YGX was found using an ablation setting of 3 J cm^{-2} – 5Hz). (a–d) Acceptable ages were obtained for scheelite WX27 in normal ablation settings; (e and f) much younger ages were obtained for scheelite WX27 in the special ablation settings of high frequency (10 Hz) and high energy density (10 J cm^{-2}).

one analysis procedure (Fig. 2b). Four lower intercept $^{206}Pb/^{238}U$ ages of 140.1 ± 4.6 Ma (1σ, MSWD = 1.9; Fig. 2a), 141.2 ± 2.8 Ma (1σ, MSWD = 1.6; Fig. 2b), 141.8 ± 2.0 Ma (1σ, MSWD = 2.8; Fig. 2c), and 142.6 ± 1.7 Ma (1σ, MSWD = 1.7; Fig. 2d) are obtained in the Tera–Wasserburg Concordia diagram, respectively. In the special ablation setting of high energy density (10 J cm^{-2}) and high sampling rate (10 Hz), two younger ages of 130.1 ± 1.3 Ma (1σ, MSWD = 2.1; Fig. 2e) and 127.5 ± 1.6 Ma (1σ, MSWD = 2.4; Fig. 2f) were obtained in the Tera–Wasserburg Concordia diagram.

4.3 U–Pb results of scheelite WX27 calibrated by the combined calibration method in different ablation settings

Using the same normal ablation settings described above, including the low energy density (3 J cm^{-2}) and medium sampling rate (5 Hz) (Fig. 3a and b), six lower intercept $^{206}Pb/^{238}U$ ages of 144.3 ± 2.2 Ma (1σ, MSWD = 2.3; Fig. 3a), 142.7 ± 2.4 Ma (1σ, MSWD = 1.8; Fig. 3b), 137.9 ± 4.7 Ma (1σ, MSWD = 1.8; Fig. 3c), 139.9 ± 3.0 Ma (1σ, MSWD = 1.6; Fig. 3d), 139.0 ± 2.1 Ma (1σ, MSWD = 2.8; Fig. 3e), and 140.5 ± 1.5 Ma (1σ, MSWD = 1.3; Fig. 3f) are obtained in the Tera–Wasserburg Concordia diagram, respectively. In the special ablation setting of high energy density (10 J cm^{-2}) and high sampling rate (10 Hz), two younger ages of 128.8 ± 1.6 Ma (1σ, MSWD = 2.6; Fig. 3g) and 128.2 ± 1.7 Ma (1σ, MSWD = 2.3; Fig. 3h) were obtained in the Tera–Wasserburg Concordia diagram.

4.4 U–Pb results of scheelite WX27 calibrated by using NIST612 in different ablation settings

Using the normal ablation settings of low to medium energy densities (3–5 J cm^{-2}) and medium–high sampling rates (5–10 Hz), four younger lower intercept $^{206}Pb/^{238}U$ ages of 117.5 ± 1.1 Ma (1σ, MSWD = 1.2; Fig. 4a), 118.0 ± 2.1 Ma (1σ, MSWD = 2.0; Fig. 4b), 119.6 ± 4.1 Ma (1σ, MSWD = 1.8; Fig. 4c), and 126.3 ±

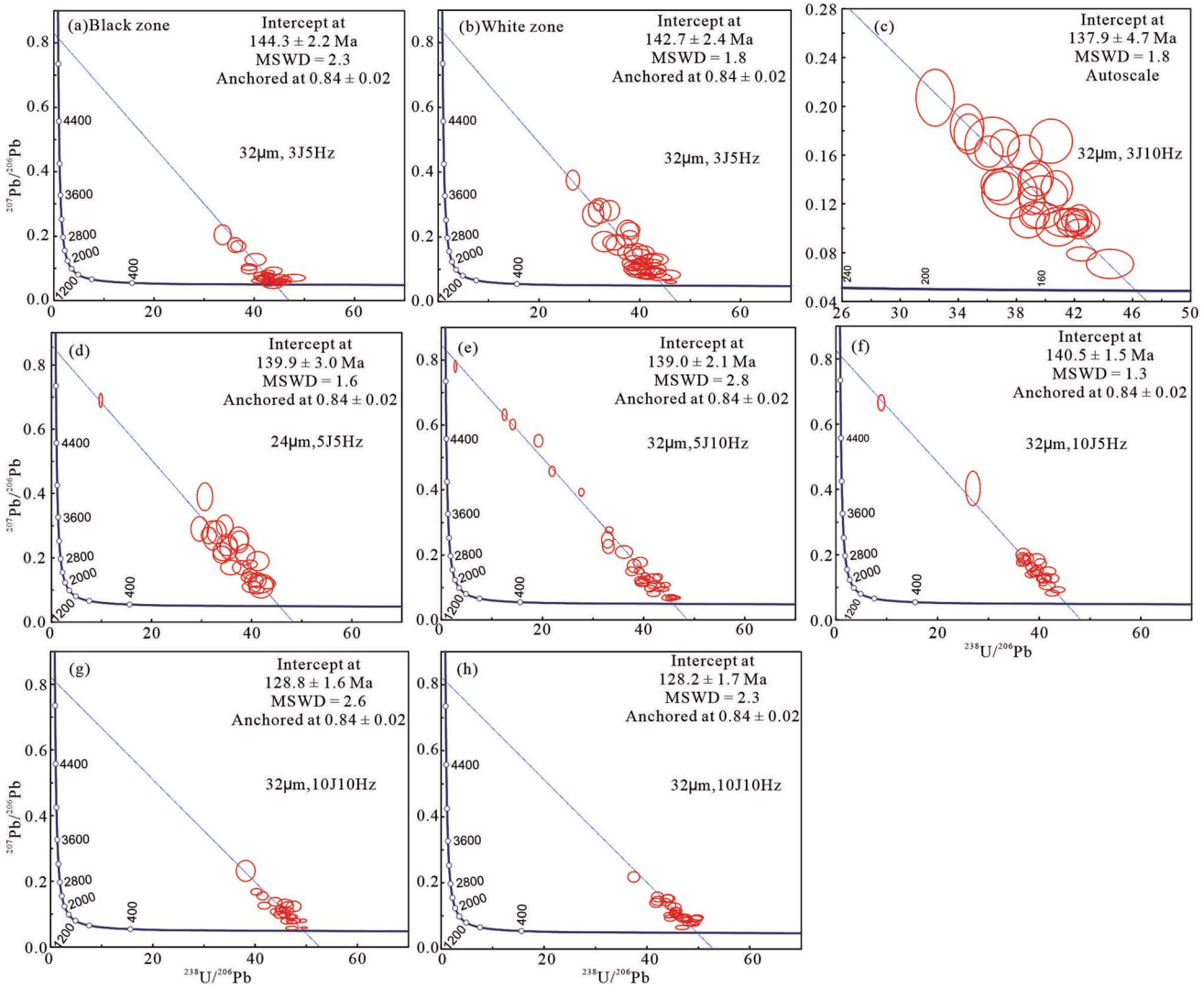

Fig. 3 *In situ* U–Pb ages of scheelite WX27 calibrated by the combined calibration method (NIST612 for $^{207}Pb/^{206}Pb$ and wolframite YGX for $^{238}U/^{206}Pb$ ratios, respectively) in different ablation settings. (a–f) All the ages are acceptable and consistent with the published and unpublished mineralization ages (144.8 ± 11.7 and 141.8 ± 5.3 Ma) within error; (g and h) two much younger ages of 128.8 ± 1.6 and 128.2 ± 1.7 Ma were obtained for scheelite WX27 using the condition of high frequency (10 Hz) and high energy density (10 J cm^{-2}).

1.9 Ma (1σ, MSWD = 2.8; Fig. 4e) are obtained in the Tera–Wasserburg Concordia diagram, respectively. A slightly younger age of 134.9 ± 3.1 Ma (1σ, MSWD = 1.8; Fig. 4d) was obtained when using a small spot-size of 24 μm in an analysis procedure.

Three acceptable ages of 142.8 ± 2.0 Ma (1σ, MSWD = 1.6; Fig. 4f), 140.2 ± 1.9 Ma (1σ, MSWD = 3.0; Fig. 4g), and 140.9 ± 1.8 Ma (1σ, MSWD = 2.3; Fig. 4h) were obtained in the Tera–Wasserburg Concordia diagram, when using the special ablation setting of high energy density (10 J cm^{-2}) and medium–high sampling rates (5–10 Hz).

4.5 Application of scheelite *in situ* U–Pb dating for five typical W deposits

(1) The Baiganhu W–Sn ore district. The early stage of scheelite KA: forty-three and thirty spots contain U concentrations varying from 2.0 to 79.9 and 1.0 to 35.7 ppm (averaging 24.4 and 15.3 ppm, respectively) and total Pb concentrations ranging from 13.0 to 77.0 and 10.7 to 20.4 ppm (averaging 30.1 and 14.0 ppm, respectively) (Table S-3†), respectively. Lower intercept $^{206}Pb/^{238}U$ ages of 432 ± 17 (1σ, MSWD = 0.7; Fig. 5a) and 423.0 ± 17 Ma (1σ, MSWD = 1.3; Fig. 5d) are obtained in the Tera–Wasserburg Concordia diagram, respectively.

The late stage of scheelite KA: eighty and forty-six spots have U concentrations ranging from 0.9 to 36.6 and 0.7 to 49.5 ppm (averaging 9.8 and 20.7 ppm, respectively) and total Pb concentrations ranging from 7.5 to 41.3 and 8.6 to 32.1 ppm (averaging 18.3 and 16.7 ppm, respectively) (Table S-3†), respectively. Two lower intercept $^{206}Pb/^{238}U$ ages of 376.4 ± 9.5 (1σ, MSWD = 1.2; Fig. 5b) and 381 ± 11 Ma (1σ, MSWD = 2.1; Fig. 5e) are obtained in the Tera–Wasserburg Concordia diagram, respectively.

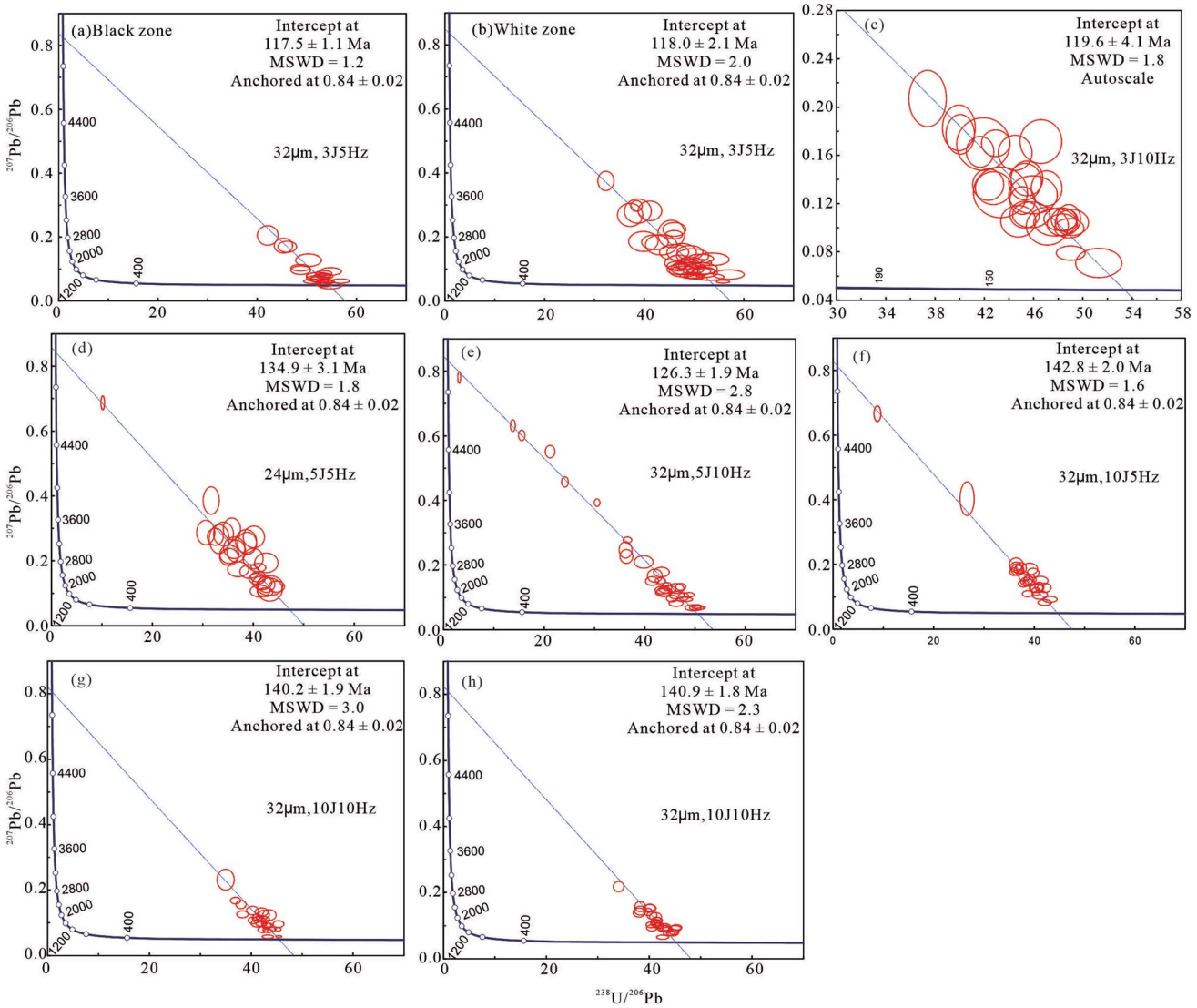

Fig. 4 U–Pb ages of scheelite WX27 calibrated by using NIST612 for both $^{207}Pb/^{206}Pb$ and $^{238}U/^{206}Pb$ ratios in different ablation settings. (a–c and e) Much younger ages were obtained for scheelite WX27 in normal ablation settings; (d) a slightly younger age was obtained for scheelite WX27 using a small spot size of 24 μm and medium frequency (5 Hz) and energy density (5 J cm^{-2}); (f–h) acceptable ages were obtained for scheelite WX27 when using the special conditions of high energy density (10 J cm^{-2}) and mid-high frequency (5–10 Hz).

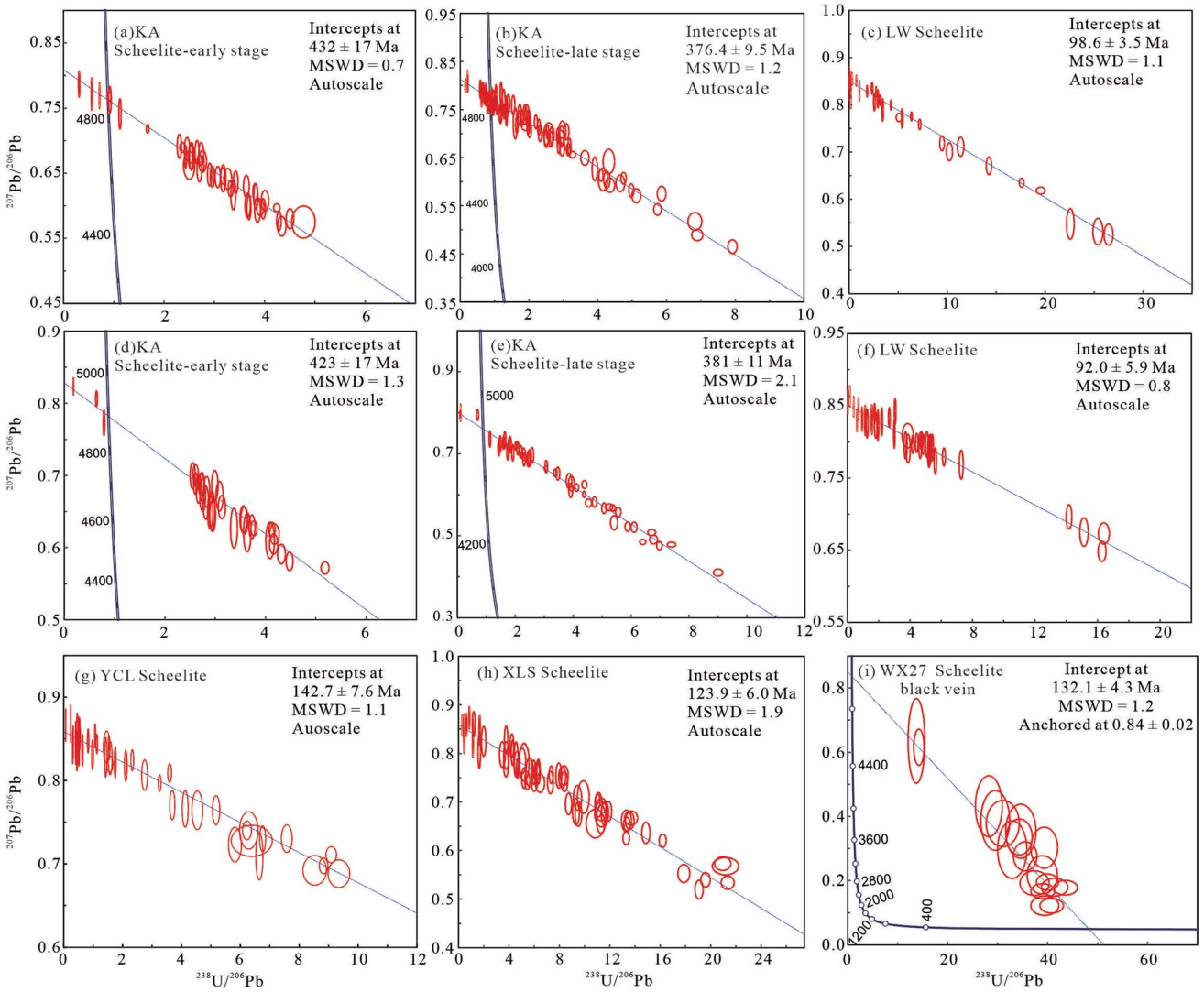

Fig. 5 Lower intercept $^{206}Pb/^{238}U$ ages for scheelite samples from five typical W deposits (calibrated by the combined calibration method). (a–c) The scheelite samples of KA and LW were analyzed in different analyzed procedures; (d–f) the scheelite KA and LW with three ages of 423 ± 17, 381 ± 11, and 92.0 ± 5.9 Ma were analyzed and calibrated in the same analyzed procedure. Highlights: except 376.4 ± 9.5 and 381 ± 11 Ma for scheelite KA in the late stage, and 132.1 ± 4.2 Ma for the late black vein of WX27, all other ages are consistent with the published mineralization age within error for each W deposit.

(2) The Luowei W polymetallic deposit. Thirty-one and thirty-nine spots from scheelite LW contain U concentrations varying from 0.002 to 153.1 ppm and 0.2 to 76.0 (averaging 33.0 and 16.9 ppm, respectively) and total Pb concentrations varying from 3.6 to 27.3 and 8.3 to 14.4 ppm (averaging 12.4 and 10.7 ppm, respectively) (Table S-3†), respectively. Two groups of data obtain two lower intercept $^{206}Pb/^{238}U$ ages of 98.6 ± 3.5 (1σ, MSWD = 1.1; Fig. 5c) and 92.0 ± 5.9 Ma (1σ, MSWD = 0.8; Fig. 5f) in the Tera–Wasserburg Concordia diagram, respectively.

(3) The Yangchuling porphyry W–Mo deposit. Forty-two spots from sample YCL have U concentrations ranging from 0.2 to 43.3 ppm (averaging 12.9 ppm) and total Pb concentrations ranging from 9.5 to 13.8 ppm (averaging 11.6 ppm) (Table S-3†). These spots obtain a lower intercept $^{206}Pb/^{238}U$ age of 142.7 ± 7.6 (1σ, MSWD = 1.1; Fig. 5g) in the Tera–Wasserburg Concordia diagram.

(4) The Xianglushan skarn W deposit. Sixty-one spots from scheelite XLS contain U concentrations ranging from 0.2 to 45.1 ppm (averaging 12.3 ppm) and total Pb concentrations ranging from 2.1 to 5.8 ppm (averaging 3.9 ppm) (Table S-3†). A lower intercept $^{206}Pb/^{238}U$ age of 123.9 ± 6.0 (1σ, MSWD = 1.9; Fig. 5h) is obtained in the Tera–Wasserburg Concordia diagram.

(5) The Woxi W–Sb–Au deposit. Twenty-six, thirty-eight, and eighteen spots from the black and white zones and the black vein in scheelite WX27 have U concentrations ranging from 3.4 to 22.3, 2.6 to 24.6, and 0.3 to 7.2 ppm, with an average value of 12.4, 8.4, and 3.4 ppm, respectively (Tables S-2 and S-3†). Their total Pb concentrations are very low and range from 0.2 to 0.5, 0.1 to 0.8, and 0.1 to 0.4 ppm with an average value of 0.3, 0.3, and 0.3 ppm, respectively. The data of twenty-six, thirty-eight,

and eighteen spots yield lower intercept $^{206}Pb/^{238}U$ ages of 144.3 ± 2.2 (1σ, MSWD = 2.3; Fig. 3a), 142.7 ± 2.4 (1σ, MSWD = 1.8; Fig. 3b), and 132.1 ± 4.3 (1σ, MSWD = 1.2; Fig. 5i) anchored at an initial $^{207}Pb/^{206}Pb$ value of 0.84 ± 0.02 from Luo *et al.*[42] in the Tera–Wasserburg Concordia diagram, respectively.

5. Discussion

5.1 Matrix effect between scheelite and wolframite in different ablation settings

Several tungstate minerals were analyzed as reliable geochronometers to constrain W-related mineralization events.[1,10,17–20,23] Ferberite, hübnerite, and wolframite were confirmed to get accurate and precise *in situ* U–Pb ages when using the well-characterized wolframite sample YGX as a primary standard[17] or the combined calibration method.[21] Meanwhile, scheelite as a useful geochronometer to directly date the W mineralization event was also proposed.[14,15] However, the reliability of this U–Pb dating technique for scheelite has not been evaluated due to the lack of matrix-matched reference material. Furthermore, the analysis of the matrix effect between wolframite and scheelite samples may improve the *in situ* U–Pb dating technique for tungstate minerals.

The apatite sample intergrowth with scheelite sample WX27 was dated by LA-SF-ICP-MS and calibrated by using apatite OD306.[30] The known Qinghu and MAD apatites were used as the secondary standards and obtained the ages of 163.3 ± 2.6 and 480.1 ± 4.9 Ma, respectively, indicating that the obtained U–Pb age of 141.8 ± 5.3 Ma is reliable for this apatite sample. Moreover, this age is also consistent with the known age of 144.8 ± 11.7 Ma for the Woxi W–Sb–Au deposit.[29] Meanwhile, several acceptable ages were also obtained for this deposit *via in situ* U–Pb dating of wolframite and a low common-lead scheelite sample WX27 (Fig. 2a–d and 3a–f). Combined with its detailed CL images for all grains to avoid the micro-late-black vein (Fig. 1), this sample was utilized as a candidate reference material to validate the calibrated ages for approach analysis together with a well-characterized wolframite sample YGX.

For *in situ* U–Pb dating of zircon, apatite, titanite, garnet, cassiterite, and wolframite, low to medium energy densities (3–5 J cm^{-2}) and medium–high sampling rates (5–10 Hz) and large crater diameters of >30 μm were commonly used for minimizing the element and isotopic fractionation to reduce the matrix effect between the matrix-matched minerals.[17,21,30,43–46] However, for low-U and -Pb minerals (*e.g.*, calcite), high energy densities and sampling rates were proposed to enhance sensitivity.[47]

In our analysis, scheelite WX27 has been accurately determined using the normal ablation settings of 3 J cm^{-2} – 5 Hz, 3 J cm^{-2} – 10 Hz, 5 J cm^{-2} – 5 Hz, 5 J cm^{-2} – 10 Hz, and 10 J cm^{-2} – 5 Hz. All the lower intercept $^{206}Pb/^{238}U$ ages are consistent with each other within error (Fig. 2a–d and 3a–f), no matter whether they were calibrated by using concordant wolframite YGX or the combined calibration method (NIST612 for $^{207}Pb/^{206}Pb$ and YGX for $^{238}U/^{206}Pb$ ratios). Even a small spot size of 24 μm combined with the medium energy densities and sampling rates (5 J cm^{-2} – 5 Hz) was used to slightly increase the matrix effect (Fig. 2b). All these ages agree with two known ages from the Woxi deposit with age offsets of <3.8% (Table 2). Moreover, the combined calibration method was applied to constrain the formation age for five typical W deposits and the obtained age agrees well with the known ages within error from each W deposit (Table 3 and Fig. 5). Both of these results indicate that there is no matrix effect between wolframite and scheelite using single spot analysis mode in normal ablation settings. When using a special ablation setting of high energy density and sampling rate (10 J cm^{-2} – 10 Hz), two quite younger ages were obtained for scheelite WX27 with age offsets of >9.2% relative to the average value of two known ages (Fig. 2e, f, 3g, h and Table 2), no matter which calibration method mentioned above was used, indicating that the matrix effect between wolframite and scheelite increases obviously in this situation.

All those ages above calibrated by the two calibration methods under normal ablation conditions are consistent with

Table 2 *In situ* U–Pb ages of scheelite sample WX27 calibrated by three methods in different ablation settings[a]

	Age (Ma)			
Ablation settings	Calibrated by using concordant wolframite YGX	Calibrated by the combined calibration method	Calibrated by using NIST612	Age offset (%)
32 μm – 3 J cm^{-2} – 5 Hz		144.3	117.5	0.7, 18.0
		142.7	118.0	0.4, 17.7
32 μm – 3 J cm^{-2} – 10 Hz	140.1	137.9	119.6	2.2, 3.8, 16.5
24 μm – 5 J cm^{-2} – 5 Hz	141.2	139.9	134.9	1.5, 2.4, 5.9
32 μm – 5 J cm^{-2} – 10 Hz	141.8	139.0	126.3	1.0, 3.0, 11.9
32 μm – 10 J cm^{-2} – 5 Hz	142.6	140.5	142.8	0.5, 2.0, 0.3
32 μm – 10 J cm^{-2} – 10 Hz	130.1	128.8	140.2	9.2, 10.1, 2.2
	127.5	128.2	140.9	11.0, 10.5, 1.7

[a] The uncertainty of age is not considered for calculation of the age offset, which is calculated using the mathematical equation abs($A - B$))/$A \times 100$; A is the average value of two ages for the Woxi deposit, *i.e.*, $A = 1/2 \times (144.8 + 141.8) = 143.3$.

Table 3 Acceptable *in situ* U–Pb ages of scheelite samples from five typical W deposits (calibrated by the combined calibration method)

		Mineralization ages from previous studies		Age (Ma)	
Scheelite	Deposit	Ages	Methods and references	Early stage	Late stage
KA	Baiganhu W–Sn deposit	425.9 ± 4.3, 427.6 ± 5.1, 429.2 ± 6.8, and 427 ± 13	*In situ* cassiterite and wolframite U–Pb ages[21,32]	432 ± 17, 423 ± 17	376.4 ± 9.5, 381 ± 11
LW	Luowei W polymetallic deposit	92 ± 3, 93 ± 3, and 95.9 ± 1.7	Muscovite $^{40}Ar/^{39}Ar$ and molybdenite Re–Os ages[36]	98.6 ± 3.5, 92.0 ± 5.9	
YCL	Yangchuling porphyry W deposit	144.9 ± 0.7 and 146.4 ± 1.0 Ma	Molybdenite Re–Os ages[38,39]	142.7 ± 7.6	
XLS	Xianglushan skarn W deposit	121 ± 11, 122.8 ± 0.8, and 125.5 ± 0.7	Scheelite Sm–Nd,[40] muscovite $^{40}Ar/^{39}Ar$ and molybdenite Re–Os ages[41]	123.9 ± 6.0	
WX27	Woxi W–Sb–Au deposit	144.8 ± 11.7 and 141.8 ± 5.3 Ma	Rb–Sr isochronal age of fluid inclusions in quartz[29] and our unpublished *in situ* apatite U–Pb age	144.3 ± 2.2, 142.7 ± 2.4	132.1 ± 4.3

each other as well as with two known ages of the Woxi deposit within error, confirming that both the calibration methods for *in situ* U–Pb dating of scheelite are reliable. Variable U and common Pb in wolframite YGX were identified in previous and our studies.[17,23] Therefore, the different grains of wolframite YGX are not always concordant due to its inhomogeneity, and thus the combined calibration method can also be used as a reliable supplement for the method of using concordant wolframite YGX as the primary standard.

5.2 The reliability of the calibration method using NIST glasses as primary standards

NIST glasses were used as the primary standard for *in situ* U–Pb or Th–Pb dating of allanite,[7] cassiterite,[9] monazite,[10] xenotime,[10] zircon,[11,48] and scheelite.[14,15,49] However, this calibration method was not adequately evaluated and difficult to follow. There commonly exist significant matrix effects between NIST glasses and natural minerals unless using the special analytical conditions, which still depend on different laboratories and accessory minerals, *e.g.*, keeping the $^{206}Pb/^{238}U$ ratio of NIST 610 at ~0.22 in the whole experimental process to accurately date cassiterite,[43] adding some water vapor by using special equipment into the ablation cell to maintain the accuracy of Th–Pb dating for monazite and xenotime,[44] and using certain operating conditions to keep the loss of Pb and the retention of U within the crater equal to get accurate age for zircons.[11]

In this analysis, the geochronological data of samples WX27 were calibrated again by using NIST612 for comparison. Using all the different ablation settings, only three ages of 142.8 ± 2.0, 140.2 ± 1.9, and 140.9 ± 1.8 Ma (Fig. 4f–h) are consistent with the known ages within error, and the others are much younger, with age offsets ranging from 5.9% to 18.0% (Fig. 4 and Table 2). Thus, inaccurate ages were often obtained when using NIST612 as the primary standard unless using the special ablation settings of high energy density (10 J cm^{-2}) and mid-high sampling rates (5–10 Hz) to keep the loss of Pb and the retention of U within the crater equal as reported in a previous study.[11] Collectively, NIST glasses are not suitable as a primary standard for *in situ* U–Pb dating of scheelite under normal analyzed conditions.

6. Conclusions

(1) A robust age can be obtained by LA-SF-ICP-MS U–Pb dating of scheelite using concordant wolframite YGX as the primary standard or the combined calibration method using single spot analysis mode in normal ablation settings.

(2) There is no significant matrix effect between scheelite and wolframite for *in situ* U–Pb dating using single spot analysis mode in normal ablation settings.

(3) NIST glasses are commonly not suitable as a primary standard for *in situ* U–Pb dating of scheelite.

(4) Scheelite WX27 contains low common lead and can be utilized as a candidate reference material to validate the calibrated ages for *in situ* U–Pb dating of scheelite at the moment.

Conflicts of interest

There are no conflicts of interest to declare.

Acknowledgements

This study was financially supported by the National Key Research and Development Program of China (Grant No. 2018YFA0702602), the National Natural Science Foundation of China (Grant No. 42072103), and Youth Innovation Promotion Association, Chinese Academy of Sciences (No. 2020393). The authors are thankful to Dr Ya'nan Zhu, Zhen Zheng, and Shiwen Yang for providing scheelite samples, and are also thankful to Dr Shaohua Dong for helping them record CL images.

References

1 R. Eichhorn, R. Höll, E. Jagout and U. Schärer, *Geochim. Cosmochim. Acta*, 1997, **61**, 5005–5022.

2 Z. Yang, R. C. Wang, W. L. Zhang, Z. Y. Chu, J. Chen, J. C. Zhu and R. Q. Zhang, *Sci. China: Earth Sci.*, 2014, **57**, 1551–1566.
3 Z. J. Guo, J. W. Li, X. Y. Xu, Z. Y. Song and X. Z. Dong, *Lithos*, 2016, **261**, 307–321.
4 S. B. Liu, Z. Q. Liu, C. H. Wang, D. H. Wang, Z. Zhao and Z. H. Hu, *Earth Sci. Front.*, 2017, **24**, 17–30.
5 C. Chen, Y. S. Ren, T. T. Wu, Q. Yang and Q. Q. Shang, *Geol. J.*, 2019, **54**, 639–655.
6 S. D. Yuan, J. T. Peng, S. Hao, H. M. Li, J. Z. Geng and D. L. Zhang, *Ore Geol. Rev.*, 2011, **43**, 235–242.
7 C. R. M. McFarlane, *Chem. Geol.*, 2016, **438**, 91–1028.
8 M. Burn, P. Lanari, T. Pettke and M. Engi, *J. Anal. At. Spectrom.*, 2017, **32**, 1359–1377.
9 Y. B. Cheng, C. Spandler, A. Kemp, J. W. Mao, B. Rusk, Y. Hu and K. Blake, *Am. Mineral.*, 2019, **104**, 118–129.
10 T. Luo, X. D. Deng, J. W. Li, Z. C. Hu, W. Zhang, Y. S. Liu and J. F. Zhang, *J. Anal. At. Spectrom.*, 2019, **34**, 1439–1446.
11 B. K. Kuhn, K. Birbaum, Y. Luo and D. Günther, *J. Anal. At. Spectrom.*, 2010, **25**, 21–27.
12 S. E. Jackson, N. J. Pearson, W. L. Griffin and E. A. Belousova, *Chem. Geol.*, 2004, **211**, 47–69.
13 E. P. Corbett, A. Simonetti, P. Shaw, L. Corcoran, Q. G. Crowley and B. C. Hoare, *Chem. Geol.*, 2020, 119568.
14 N. E. Wintzer, V. S. Gillerman and M. D. Schmitz, *GSA Annual Meeting in Denver*, Colorado, USA, 2016.
15 T. Poitrenaud, M. Poujol, R. Augier and E. Marcoux, *Miner. Deposita*, 2020, **55**, 1127–1147.
16 M. Ghaderi, J. Michael Palin, I. H. Campbell and P. J. Sylvester, *Econ. Geol.*, 1999, **94**, 423–437.
17 M. Yang, Y. H. Yang, S. T. Wu, R. L. Romer, X. D. Che, Z. F. Zhao, W. S. Li, J. H. Yang, F. Y. Wu, L. W. Xie, C. Huang, D. Zhang and Y. Zhang, *J. Anal. At. Spectrom.*, 2020, **35**, 2191–2203.
18 M. Harlaux, R. L. Romer, J. Mercadier, C. Morlot, C. Marignac and M. Cuney, *Miner. Deposita*, 2018, **53**, 21–51.
19 P. A. Carr, J. Mercadier, M. Harlaux, R. L. Romer, E. Moreira, H. Legros, M. Cuney, C. Marignac, J. Cauzid, L. Salsi, A. Lecomte, O. Rouer and C. Peiffert, *Chem. Geol.*, 2021, **584**, 120511.
20 P. Lecumberri-Sanchez, R. L. Romer, V. Lüders and R. J. Bodnar, *Miner. Deposita*, 2014, **49**, 353–369.
21 Y. W. Tang, K. Cui, Z. Zheng, J. F. Gao, J. J. Han, J. H. Yang and L. Liu, *Gondwana Res.*, 2020, **83**, 217–231.
22 Y. W. Tang, J. F. Gao, T. G. Lan, K. Cui, J. J. Han, X. Zhang, Y. W. Chen and Y. H. Chen, *Ore Geol. Rev.*, 2021, **130**, 103970.
23 X. D. Deng, T. Luo, J. W. Li and Z. C. Hu, *Chem. Geol.*, 2019, **515**, 94–104.
24 X. Y. Zhu, J. B. Wang, Y. L. Wang, X. Y. Cheng, Q. B. Fu, M. Fu and Z. F. Yu, *Geol. Explor.*, 2014, **50**, 947–960.
25 C. H. Xiao, H. Liu, Y. K. Shen, C. S. Wei, X. W. Le, D. G. Ou and L. Zhang, *Miner. Deposits*, 2018, **37**, 1037–1051.
26 J. S. Stacey and J. D. Kramers, *Earth Planet. Sci. Lett.*, 1975, **26**, 207–221.
27 Y. S. Liu, Z. C. Hu, K. Q. Zong, C. G. Gao, S. Gao, J. Xu and H. H. Chen, *Chin. Sci. Bull.*, 2010, **55**, 1535–1546.
28 T. Luo, H. Zhao, Q. L. Li, Y. Li, W. Zhang, J. L. Guo, Y. S. Liu, J. F. Zhang and Z. C. Hu, *Geostand. Geoanal. Res.*, 2020, **44**, 653–668.
29 M. K. Shi, B. Q. Fu, X. X. Jin and X. C. Zhou, *Antimony Metallogeny in the Central Part of Hunan Province*, Hunan Science & Technology Press, Changsha, 1993, in Chinese.
30 J. Thompson, S. Meffre, R. Maas, V. Kamenetsky, M. Kamenetsky, K. Goemann, K. Ehrig and L. Danyushevsky, *J. Anal. At. Spectrom.*, 2016, **31**, 1206–1215.
31 X. H. Li, G. Q. Tang, B. Gong, Y. H. Yang, K. J. Hou, Z. C. Hu, Q. L. Li, Y. Liu and W. X. Li, *Chin. Sci. Bull.*, 2013, **58**, 4647–4654.
32 Y. B. Gao, W. Y. Li, Z. M. Li, J. Wang, K. Hattori, Z. W. Zhang and J. Z. Geng, *Econ. Geol.*, 2014, **109**, 1787–1799.
33 C. Y. Feng, G. C. Li, D. X. Li, A. S. Zhou and H. M. Li, *Miner. Deposits*, 2013, **32**, 207–216.
34 Z. Zheng, Y. J. Chen, X. H. Deng, S. W. Yue and H. J. Chen, *Geol. China.*, 2016, **43**, 1341–1352.
35 G. C. Li, C. Y. Feng, R. J. Wang, S. C. Ma, H. M. Li and A. S. Zhou, *Diqiu Xuebao*, 2012, **33**, 216–226.
36 Y. Y. Feng, W. Fu, Z. H. Feng, J. W. Yang, Z. Y. Li, X. W. Le, S. S. Li, M. Feng, C. Z. Wang and J. F. Xu, *Ore Geol. Rev.*, 2021, 103932.
37 C. H. Xiao, Y. K. Shen, C. S. Wei, X. K. Su, X. W. Le and L. Zhang, *Geoscience*, 2018, **32**, 289–304.
38 Q. Q. Zeng, Z. H. Hu, X. G. Wang, L. X. Gong, L. M. Nie and Q. Li, *Geol. China*, 2019, **46**, 841–849.
39 J. W. Mao, B. K. Xiong, J. Liu, P. Franco, Y. B. Cheng, H. S. Ye, S. W. Song and P. Dai, *Lithos*, 2017, **286–287**, 35–52.
40 J. J. Zhang, Y. P. Mei, D. H. Wang and H. Li, *Acta Geol. Sin.*, 2008, **82**, 927–931.
41 P. Dai, J. W. Mao, S. H. Wu, G. Q. Xie and X. H. Luo, *Ore Geol. Rev.*, 2018, **95**, 1161–1178.
42 J. Luo, P. Du, L. L. Jia and M. Cai, *China Metal Bulletin*, 2018, **4**, 123–124.
43 C. M. Allen and I. H. Campbell, *Chem. Geol.*, 2012, **332–333**, 157–165.
44 E. Marillo-Sialer, J. Woodhead, J. Hergt, A. Greig, M. Guillong, A. Gleadow, N. Evans and C. Paton, *J. Anal. At. Spectrom.*, 2014, **29**, 981–989.
45 C. Spandler, J. Hammerli, P. Sha, H. Hilbert-Wolf, Y. Hu, E. Roberts and M. Schmitz, *Chem. Geol.*, 2016, **425**, 110–126.
46 R. Q. Zhang, J. J. Lu, B. Lehmann, C. Y. Li, G. L. Li, L. P. Zhang, J. Guo and W. D. Sun, *Ore Geol. Rev.*, 2017, **82**, 268–284.
47 N. M. W. Roberts, E. T. Rasbury, R. R. Parrish, C. J. Smith, M. S. A. Horstwood and D. J. Condon, *Geochem., Geophys., Geosyst.*, 2017, **18**, 2807–2814.
48 T. Hirata and R. W. Nesbitt, *Geochim. Cosmochim. Acta*, 1995, **59**, 2491–2500.
49 N. E. Wintzer, *A dissertation of N. E. Wintzer in December*, School of the Environment, Washington State University, 2019, pp. 178–206.

